Goda, K. (2015). Effects of seabed surface rupture versus buried rupture on tsunami wave modeling: A case study for the 2011 Tohoku, Japan earthquake. Bulletin of the Seismological Society of America, 105(5), 2563-2571. DOI: 10.1785/0120150091

THE SEISMOLOGICAL SOCIETY OF AMERICA
400 Evelyn Ave., Suite 201
Albany, CA 94706-1375
(510) 525-5474; FAX (510) 525-7204
www.seismosoc.org

Bulletin of the Seismological Society of America, Vol. 105, No. 5, pp. –, October 2015, doi: 10.1785/0120150091

Ⓔ

Effects of Seabed Surface Rupture Versus Buried Rupture on Tsunami Wave Modeling: A Case Study for the 2011 Tohoku, Japan, Earthquake

by Katsuichiro Goda

Abstract Parametric investigations of tsunami wave modeling are performed to discuss an important issue related to the sensitivity of tsunami simulation results to varied top-edge depths of a shallowly dipping fault plane (seabed surface rupture versus buried fault rupture). Input boundary conditions (i.e., vertical seabed deformation) for tsunami simulation are calculated using so-called Okada equations. The analysis results for the 2011 Tohoku, Japan, tsunami case study highlight the significant effects of varied top-edge depth parameters on vertical seabed deformation and tsunami wave heights. In particular, the uplifted water outside of the fault plane for the buried rupture case, in comparison with the seabed surface-rupture case, causes large tsunami waves. The results are applicable to other tsunamigenic earthquakes that occur on a gently dipping fault plane at a shallow depth (e.g., anticipated Nankai–Tonankai earthquake) and have important implications on how tsunami inversion should be carried out and how developed source models should be interpreted.

Online Material: Figures of vertical deformation, maximum inundation height contours, and inundation height profiles.

Introduction

The goal of this article is to raise awareness on an issue regarding the use of so-called Okada (1985) equations for modeling earthquake-triggered tsunami waves. Okada formulas analytically compute seafloor deformation due to shear and tensile fault movements in an elastic half-space. In tsunami modeling, vertical deformation of ocean bottom is often substituted for initial water surface (i.e., boundary conditions for tsunami simulation), ignoring the hydrodynamic response of sea water. More rigorous approaches that account for the hydrodynamic behavior of water in response to abrupt seabed deformation are available through tsunami simulation using a nonhydrostatic, dispersive model (Yamazaki *et al.*, 2009, 2011), and filtering of (nonphysical) sharp peaks of seabed deformation (Kajiura, 1963; Gusman *et al.*, 2012; Løvholt *et al.*, 2012; Glimsdal *et al.*, 2013). Albeit simple and approximate, the substitution approach based on Okada equations is prevalent in numerous tsunami studies and is focused upon in this study.

Tsunami-hazard assessment for future scenarios involves various kinds of assumptions and approximations, as well as errors in observations and data used for model calibration. In the face of major uncertainty, assessing the sensitivity and variability of tsunami simulation results provides valuable insights into the possible ranges of tsunami-hazard estimates. The results are useful for developing robust design methods for coastal structures and tsunami-proof buildings and for planning evacuation procedures and regional land use (Federal Emergency Management Agency, 2008; Murata *et al.*, 2010). Typically, sensitivity to key earthquake source parameters is investigated by varying one feature of the earthquake source at a time while maintaining other parameters at base values. The varied parameters include fault length and width, depth to the top of the fault plane (H_{top}), dip, strike, rake, and location and amplitude of asperities (Geist, 2002; Japan Society of Civil Engineers, 2002, see Data and Resources; McCloskey *et al.*, 2008; Løvholt *et al.*, 2012; Goda *et al.*, 2014). The range of variations for these parameters should be broadly compatible with regional seismotectonic settings and may be specified by magnitude–size scaling relationships (Murotani *et al.*, 2013) and stochastic earthquake slip distributions (Mai and Beroza, 2002).

The main issue discussed in this study is related to the sensitivity of tsunami simulation results (e.g., wave profile and inundation height) to varied depths to the top of the fault plane in cases for which vertical seabed deformation is calculated using Okada equations. More specifically, I will concentrate on scenarios in which a large earthquake slip (on the order of tens of meters) occurs at shallow parts of ocean crust

along the trench on a gently dipping fault plane. A notable example of this type of events is the 2011 Tohoku, Japan, earthquake, which caused a massive tsunami (Yamazaki *et al.*, 2011; Gusman *et al.*, 2012; Satake *et al.*, 2013). Intuitively, for given fault geometry and slip distribution, one may anticipate that tsunami wave height decreases with the top-edge depth of the fault plane. However, the effects of such variations are not straightforward and depend on various factors. When the surface rupture to the seabed is assumed, Okada equations predict a discontinuous deformation profile. On the other hand, when the rupture does not reach the seabed surface and stops at a shallow depth, a continuous deformation profile with a spike is generated at an edge of rupture on a surface. This spike produces short-wavelength components. In addition, lifting sea water outside of the rupture area generates tsunami waves.

To put this in a realistic context, a case study is conducted for the 2011 Tohoku tsunami. I will show that the effects of varied top-edge depths of a fault plane (e.g., seabed surface rupture versus buried rupture) on simulated tsunami waves can be significant. An immediate situation that is relevant to the preceding problem is the anticipated **M** 9.0-class Nankai–Tonankai earthquake (Central Disaster Management Council, 2012, see Data and Resources), where the seabed surface rupture is assumed in the national tsunami model. Because there are no direct observations for source model calibration, conducting rigorous sensitivity analysis involving all assumed parameters (including the top-edge depth of the fault plane) is particularly important. Moreover, it is noteworthy that for major seismic events, various inversion studies are conducted, developing their own fault-rupture models with different fault geometry and slip distributions. In such inversion, fault geometry is usually selected prior to inversion, and a decision as to whether rupture to ocean bottom is assumed may have influence on the obtained source models. Therefore, the results related to the aforementioned issue are also relevant to tsunami inversion and thus have important implications on earthquake source characterization for future events.

This article starts with a parametric investigation of how two geometrical parameters, top-edge depth and dip angle, of a single-plane source affect the vertical deformation calculated using Okada equations. Subsequently, a real case study for the 2011 Tohoku tsunami, using an inverted source model by Satake *et al.* (2013), is discussed to highlight the influence of varied top-edge depths of the fault plane on offshore tsunami wave profiles at Global Positioning System (GPS) buoys and maximum tsunami wave heights along the coastline. This is followed by a brief discussion of implications on tsunami inversion and source characterization.

Vertical Deformation Profile Calculated by Okada Formulas: A Single-Fault-Plane Rupture

A parametric example is set up to illustrate the main problem. Consider an earthquake rupture having the following fault geometry and slip: fault length = 100 km, fault width = 50 km, strike = 180° (i.e., north–south direction; origin is at the northern end), dip = 10°, and a unit slip vector with a rake of 90°. These cases can be regarded as a typical situation for low-angle reverse-faulting earthquakes in a subduction zone. The vertical deformation at numerous locations around the fault plane is evaluated using Okada equations (the hydrodynamic response filter by Kajiura, 1963, is not taken into account).

Figure 1 shows two cases: one with rupture to seabed ($H_{top} = 0$ km) and the other with a buried fault plane ($H_{top} = 5$ km). The contour plot shows the spatial distribution of vertical deformation, and the panel below the contour shows three cross-sectional profiles of vertical deformation perpendicular to the fault strike (Fig. 1). The vertical deformation is greatest at the center of the top edge of the fault plane (cross section 1), and it decreases sharply at both ends of the fault length (cross sections 2 and 3). A remarkable difference between the cases with $H_{top} = 0$ km and $H_{top} = 5$ km is that the vertical deformation profile for $H_{top} = 0$ km is discontinuous at the strike and does not increase as the distance to the fault strike approaches zero (from the left side), whereas that for $H_{top} = 5$ km is continuous and has a peak at the fault strike. The comparison of the vertical deformation profiles for $H_{top} = 0$ and 5 km indicates that noticeable increases in vertical deformation profiles are caused near the peak along the fault strike and outside of the projected fault plane, where no vertical deformation exists for $H_{top} = 0$ km. Consequently, when deformation profiles with a buried fault plane are used in tsunami modeling, the uplifted parts (i.e., peak along the strike and outer fault-plane region) generate additional tsunami waves, in comparison with the seabed surface-rupture case.

Figure 2a shows the vertical deformation profiles (along cross section 1) for different values of H_{top} ranging from 0 to 10 km (for the same fault geometry and slip in Fig. 1). A large spike is generated along the top edge. Because the depth becomes shallower, the spike becomes sharper (the maximum height of the spike is not significantly changed), indicating that short-wavelength components tend to be generated due to the top-edge depth effects. Figure 2b shows the vertical deformation profiles (along cross section 1) for three dip angles (5°, 10°, and 20°) by considering $H_{top} = 0$ and 5 km. A notable change due to dip variations is the increased deformation at the top edge (as expected). The relative effects due to steeper dip angles on vertical deformation are different for $H_{top} = 0$ and $H_{top} = 5$ km. When the rupture to seabed is considered, the maximum vertical deformation along the fault strike increases significantly with similar discontinuous cross-sectional profiles. This indicates that the total displaced volume of water above the fault plane is changed significantly. This is not the case for the buried rupture case. The increase of the maximum vertical deformation profile at the top edge is not dramatic, having a similar cross-sectional profile. Consequently, the impact due to steeper dip angles is less pronounced for this case. Moreover, Figure 2c compares the vertical deformation profiles along cross section 1 for dip = 10° and $H_{top} = 0$ or 5 km by considering the effects of the hydrodynamic response filter by Kajiura (1963) (see

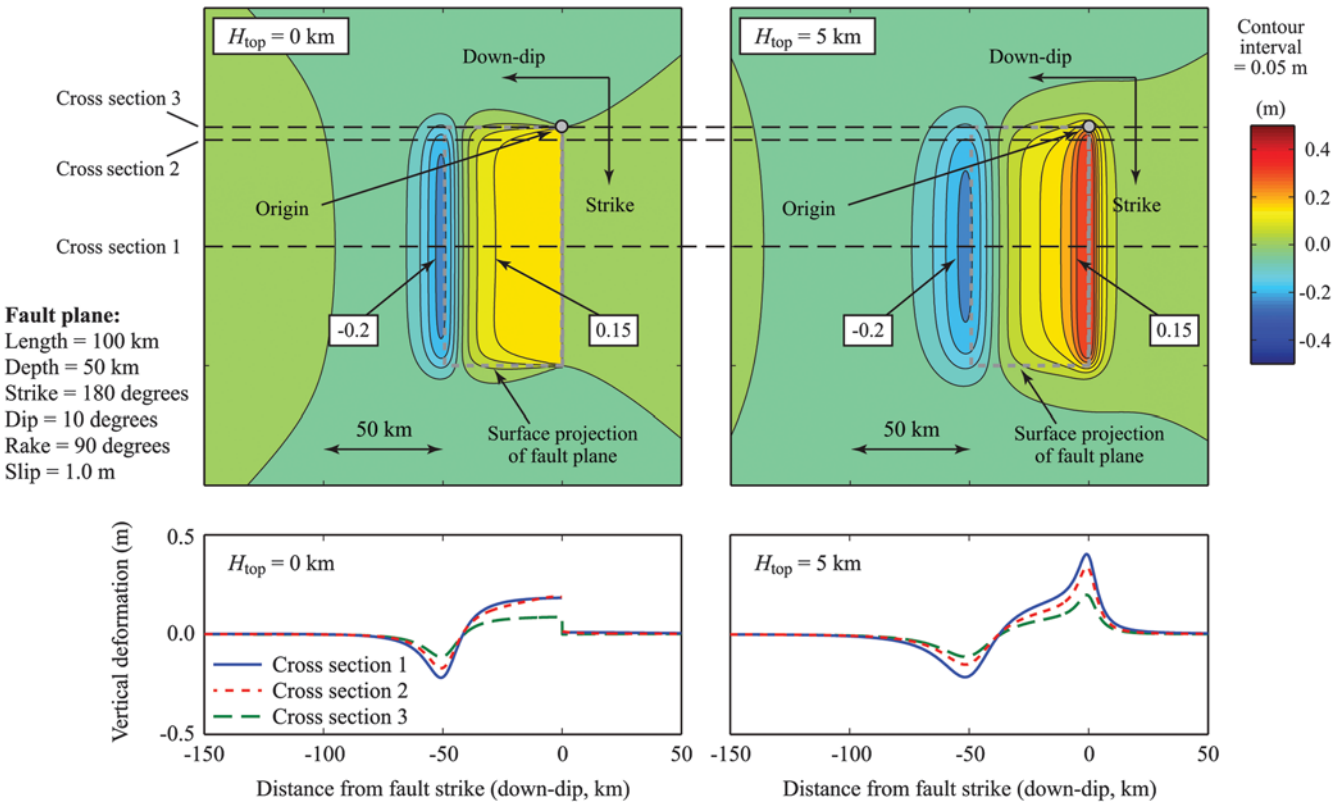

Figure 1. Vertical deformation profiles (top, contour plot; bottom, cross-sectional profiles) for two cases: (left) $H_{top} = 0$ km and (right) $H_{top} = 5$ km.

also Glimsdal *et al.*, 2013). The hydrodynamic response filter makes the vertical deformation profile smoother (and continuous even for $H_{top} = 0$ km). Notably, for the buried rupture case, the height of the peak along the top edge is decreased, whereas the uplift of water outside of the fault-rupture plane is similar. In other words, in the context of this study, the consideration of the hydrodynamic filter decreases the spike but maintains or increases the volume of the uplifted water outside of the fault-plane region.

Figures 1 and 2 suggest that caution is necessary when a large slip occurs on a gently dipping fault plane (about 5°–10°) at a shallow depth (< 10 km). When the deformation profiles are used as tsunami input, generated tsunami waves may be affected significantly. Such situations are applicable to tsunamigenic earthquakes in subduction zones.

The 2011 Tohoku Tsunami Case Study

The impact of varied top-edge depth parameters on tsunami simulation results for the 2011 Tohoku tsunami is investigated in this section. Tsunami simulation is carried out by evaluating nonlinear shallow water equations with runup using a leapfrog staggered finite-difference scheme (Goto *et al.*, 1997). Information on bathymetry, surface roughness, and coastal defense structures is obtained from the Cabinet Office of the Japanese Government (see Data and Resources). The nested grid system with a spacing of 1350 m for an offshore region and of 450 m for a near-shore and inland region is employed (the nonlinear shallow water equations are solved for the entire computational domain). At the offshore open-sea boundaries of the computational domain, outgoing tsunami waves are allowed to pass freely. On the other hand, inundation and runup calculations are performed by a moving-boundary approach at the water front, where a dry or wet condition of a computational cell is determined based on total water depth. The simulation is conducted for a duration of 2 hrs with an integration time step of 1.0 s; this duration is sufficient to simulate the most destructive parts of the tsunami waves due to the 2011 Tohoku earthquake.

To define initial boundary conditions for tsunami modeling, a source model developed by Satake *et al.* (2013) is adopted, together with the formulas by Tanioka and Satake (1996) to account for the effects of horizontal movement of the seabed on its vertical deformation. Both vertical and horizontal displacements due to earthquake slip are computed using Okada equations. Figure 3 shows the Satake *et al.* source model; there are several fault segments along the trench, having large slips exceeding 40 m. In the figure, three domains are defined: (1) trench region (enclosed by a thick rectangle), (2) down-dip region (enclosed by a polygon), and (3) outer fault-plane region (i.e., outside of the trench and down-dip regions).

The rupture model is kinematic, and its process is represented by a set of 10 slip distributions with an interval of 30 s

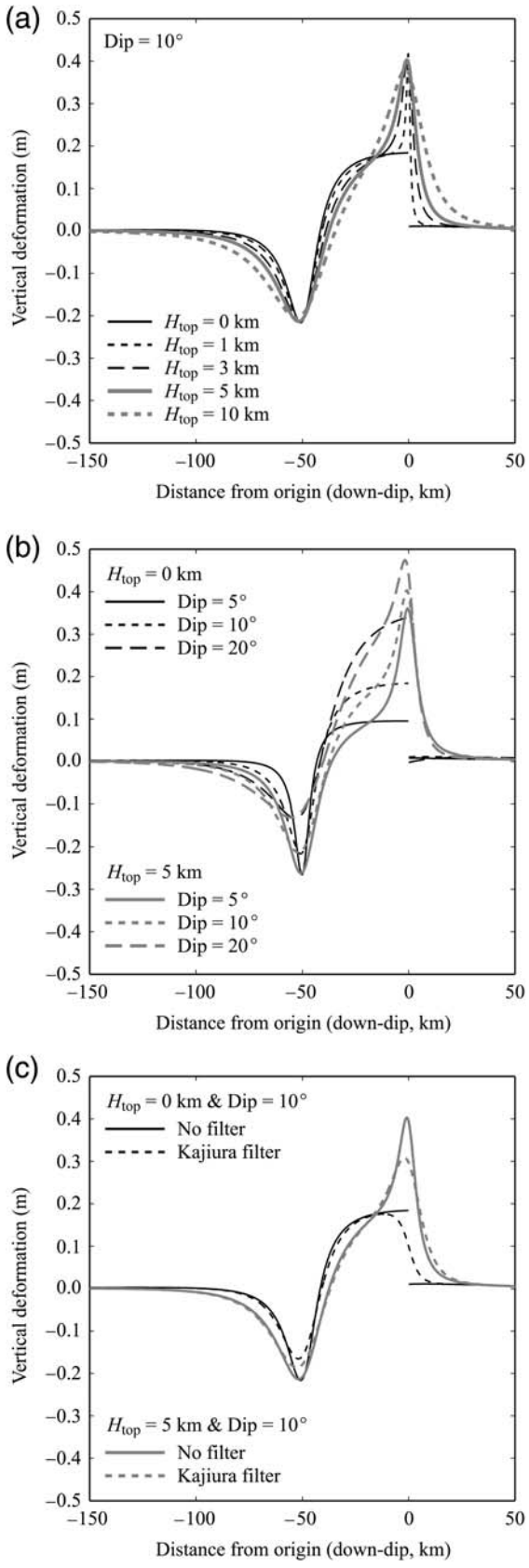

Figure 2. Comparison of vertical deformation profiles: (a) varying top-edge depths of the fault plane, (b) varying dip angles, and (c) effects of hydrodynamic filter by Kajiura (1963).

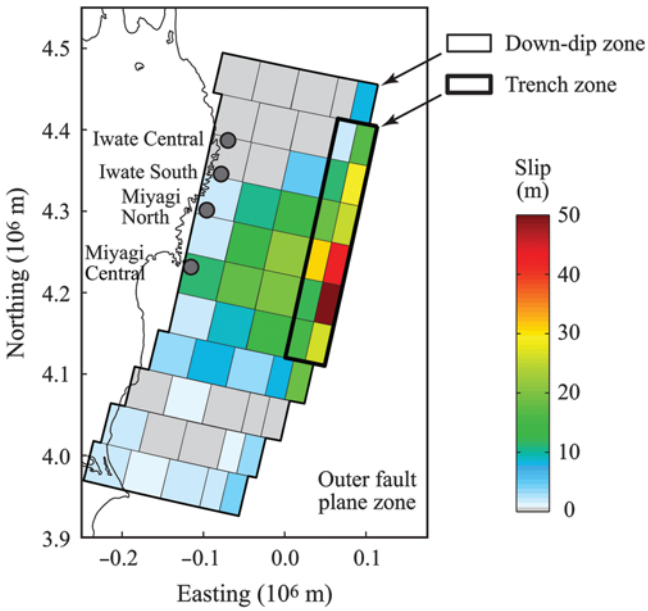

Figure 3. Source model by Satake *et al.* (2013).

(i.e., the entire rupture process takes 300 s). It is noted that the Satake *et al.* model considers the surface rupture to seabed along the trench ($H_{top} = 0$ km). To investigate the sensitivity of varied top-edge depth parameters on simulated tsunami waves, H_{top} is changed from 0 km (base case) up to 10 km; all other parameters (i.e., location, strike, dip, rake, fault geometry, and slip distribution) are not altered from the Satake *et al.* model (i.e., one-at-a-time sensitivity analysis; see Goda *et al.*, 2014, for sensitivity analysis for other parameters). The change of the top-edge depth is applied to all subfaults on the fault plane (i.e., the entire fault plane is shifted down by the indicated value of H_{top}). In this study, the effects due to variable rock rigidity on tsunami simulation (Geist and Bilek, 2001) are not taken into account to be consistent with the source inversion analysis carried out by Satake *et al.* (2013) (i.e., constant rigidity is assumed). Moreover, the hydrodynamic response filter by Kajiura (1963) is not considered, because this is not taken into account by Satake *et al.* (2013). Based on the comparison shown in Figure 2c, the observations drawn without considering the hydrodynamic response filter are generally applicable to the cases with the hydrodynamic response filter. Among the considered cases with varied depth parameters, two cases ($H_{top} = 0$ km and $H_{top} = 5$ km) are mainly discussed; Ⓔ the results for other depth cases are included in an electronic supplement to this article.

The tsunami simulation results are compared with actual observations from the 2011 Tohoku event. I focus upon measured wave profiles at four GPS buoys off the Tohoku region (i.e., Iwate Central, Iwate South, Miyagi North, and Miyagi Central, from north to south; see Fig. 3; Kawai *et al.*, 2013) and tsunami inundation heights obtained from the Tohoku Tsunami Joint Survey (TTJS) database (see Data and Resources; Mori *et al.*, 2011). It is noteworthy that the tsunami wave profiles at the four GPS buoys were used by Satake

et al. (2013) in their source inversion analysis, whereas the TTJS tsunami inundation height data were not used in the inversion. Moreover, the observed tsunami data are included in the results to provide some useful empirical reference; they are not meant for assessing the relative performance of different source models.

Figure 4a and 4b shows the vertical deformation contours for $H_{top} = 0$ km and $H_{top} = 5$ km, respectively (for concise presentation, vertical deformation values over the rupture process of 300 s are added together). In the figures, boundaries for the trench and down-dip regions are indicated by the gray broken rectangle and polygon. The deformation contour for $H_{top} = 0$ km has a sharp linear concentration of vertical deformation along the trench. On the other hand, when $H_{top} = 5$ km is considered, the boundary between the trench region and the outer region is blurred. Figure 4c shows the differences of vertical deformation contours for $H_{top} = 0$ km and $H_{top} = 5$ km and highlights the effects of the buried fault plane on vertical deformation. The increase in vertical deformation is particularly large along the trench, as well as in the outer region. For the latter, additional uplift due to the buried fault plane spreads over a relatively large distance from the trench (approximately up to 20 km).

Table 1 summarizes the displaced volumes of water in the trench zone, down-dip zone, outer fault-plane zone, and combined zone for the two cases with $H_{top} = 0$ km and $H_{top} = 5$ km. From the comparison shown in Table 1, it is clear that a large increase in the displaced volume of water occurs in the outer fault-plane region, whereas an increase in the trench region is relatively small (about 6.5%), noting that the displaced volumes of water in the trench and outer fault-plane regions are similar for the case with $H_{top} = 0$ km.

Next, the effects of top-edge depth variations on the maximum tsunami height distribution are investigated in detail. Figure 4d and 4e shows the maximum wave height contours for $H_{top} = 0$ km and $H_{top} = 5$ km, respectively. Inspection of the two contour maps indicates that the maximum tsunami wave height is increased significantly in the near-trench region as well as in the near-shore and inland region. The impact of the top-edge depth variations can be more clearly observed in Figure 4f, which displays the differences of the maximum wave height contours for the two cases. To gain further insights into which part of the increased vertical deformation in Figure 4c is responsible for the increase in the maximum tsunami wave height contour shown in Figure 4f, additional tsunami simulations are performed by separating deformation contours in the trench, down-dip, and outer regions (see Fig. 3) for the two cases with $H_{top} = 0$ km and $H_{top} = 5$ km, and then the differences of the maximum wave height contours for the two depth cases are evaluated for the three regions individually. The results are presented in Figure 4g–i. Figure 4g shows that the increased deformation in the trench region, which has significant uplift along the trench and subsidence toward the down-dip direction (see Fig. 4c), has major influence on the maximum wave height along the trench but no significant impact elsewhere. In other words, the sharp peaks due to the buried fault plane have limited effects on the near-shore tsunami wave heights, which are important from tsunami-hazard and risk assessment viewpoints. Figure 4h (i.e., down-dip region) does not show significant impact. The results shown in Figure 4i indicate that the uplift in the outer region has major impact on the maximum wave height contour. A critical factor for such a dramatic increase is due to the uplifted areas, spreading over a relatively wide spatial region. Overall, the results shown in Figure 4 clearly suggest that the issue related to the calculation of the initial tsunami profile using Okada equations is not trivial when different depths to the top of the fault plane are considered.

To further investigate the effects of the top-edge depth parameters on tsunami simulation results, wave profiles at four GPS buoys off the Tohoku region (Fig. 3) for $H_{top} = 0$ km and $H_{top} = 5$ km are compared in Figure 5. In each panel, five curves are included: the measured wave profile is shown by a thick gray line, and the wave profile simulated by taking into account vertical deformation over the entire computational domain is shown by a thin black line. The three other curves are for the simulated wave profiles computed based on vertical deformation in the trench, down-dip, and outer regions, respectively. For the base case ($H_{top} = 0$ km; Fig. 5a), measured and simulated wave profiles are in close agreement (especially Iwate South and Miyagi North). This is not surprising because Satake *et al.* (2013) used these measurements for their source inversion. The contributions of waves generated from the outer region are negligible at all four locations, and, hence, waves generated from the trench and the down-dip regions are dominant. In addition, at Iwate buoys, waves from the trench region may be considered as the single dominant source. For the buried fault-plane case ($H_{top} = 5$ km; Fig. 5b), at the Miyagi buoys (which directly face the major rupture areas of the 2011 Tohoku event; see Fig. 3), waves generated from the outer region, arriving later than those from the down-dip and trench regions, contribute significantly to the total simulated wave profiles. Consequently, the total simulated wave profiles at these buoys have delayed large peaks for $H_{top} = 5$ km, in comparison with those for $H_{top} = 0$ km. The results shown in Figure 5 corroborate the significant effects due to the uplift in the outer region, as discussed in relation to Figure 4.

Finally, Figure 6 compares the maximum tsunami inundation profiles along the Tohoku coast by considering $H_{top} = 0$ and 5 km. For comparison, the survey results (TTJS data) are included in the figure. To obtain the recorded inundation height profiles along the Tohoku coast, discrete cells, containing zero elevation, are set up along the coastline and peak values are extracted within individual cells. Note that the TTJS results are for empirical reference only; in other words, the purpose of showing Figure 6 is to compare the maximum tsunami inundation profiles for the two cases with $H_{top} = 0$ km and $H_{top} = 5$ km and is not to evaluate the relative performance of the simulation results with respect to the observations. To show the differences of the maximum

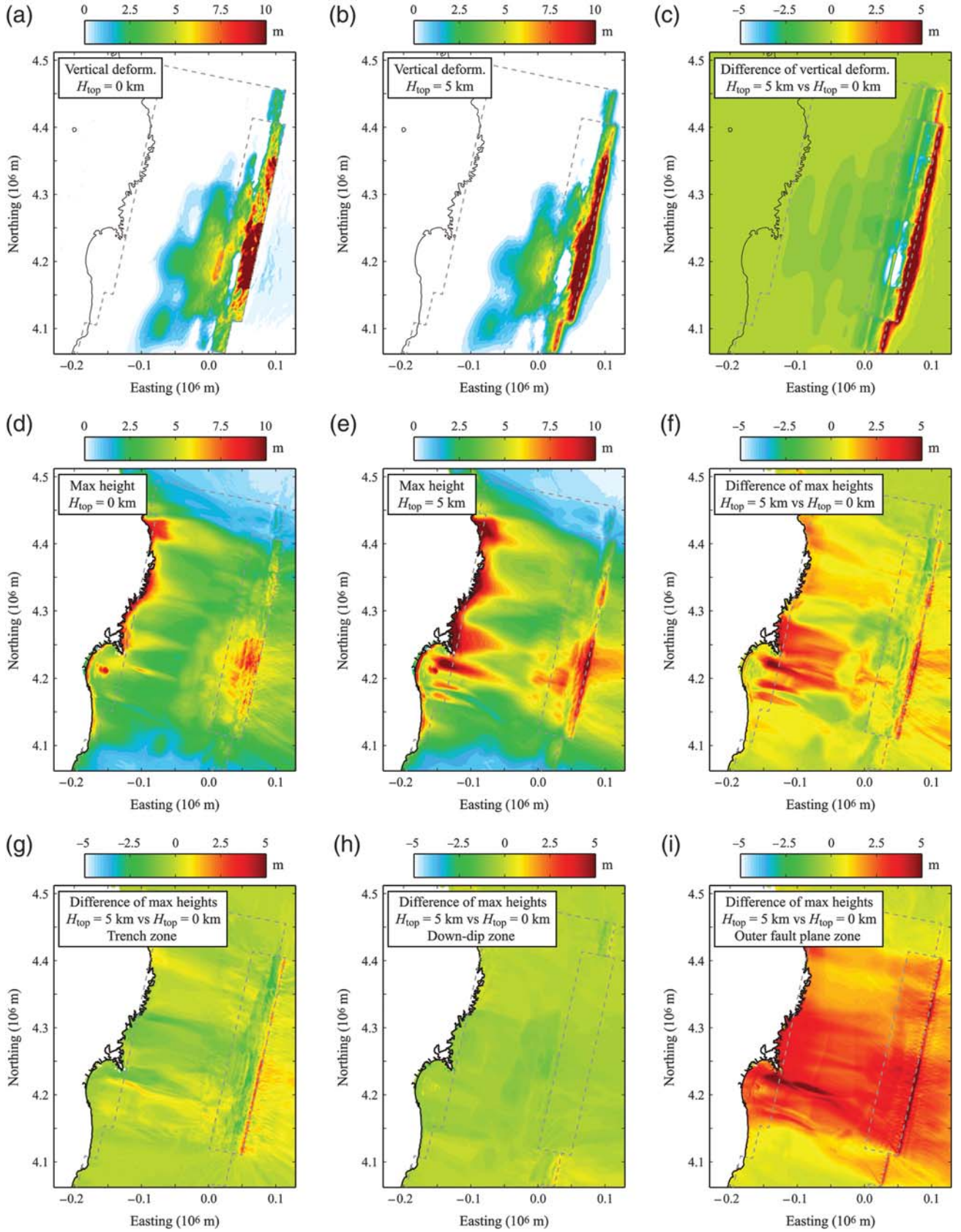

Figure 4. (a–c) Comparison of vertical deformation contours and (d–f) maximum wave heights considering two cases, $H_{top} = 0$ km and $H_{top} = 5$ km. (f) The difference of the maximum wave heights between the two cases is decomposed into those due to deformation in (g) the trench zone, (h) the down-dip zone, and (i) the outer fault plane zone.

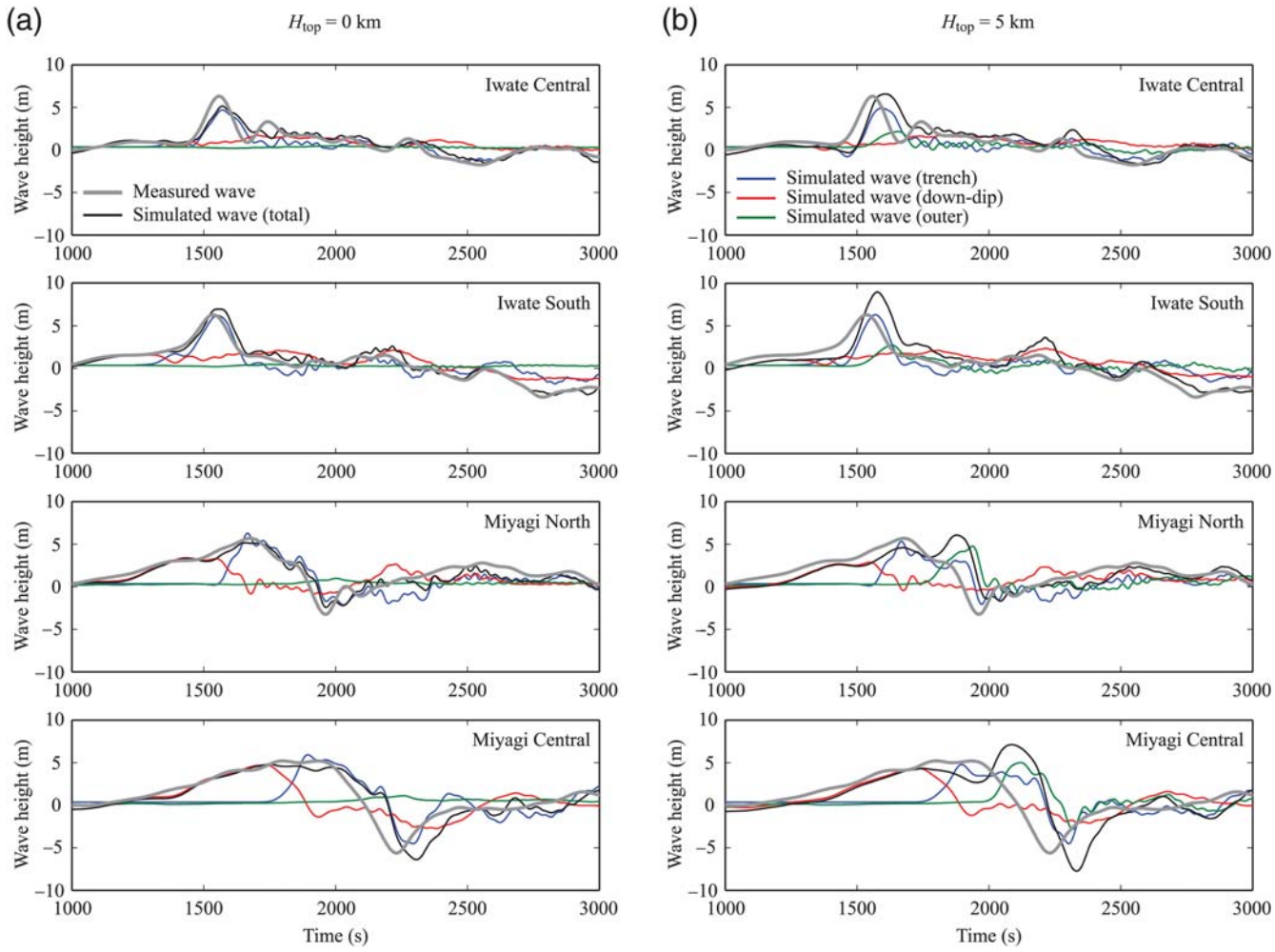

Figure 5. Tsunami wave profiles at four Global Postitioning System buoys located off the Tohoku coast by considering two cases, (a) $H_{top} = 0$ km and (b) $H_{top} = 5$ km (gray line, measured data; black line, simulated results; and others, subcomponents).

inundation profiles at regional scale, the statistics of the maximum inundation profiles (i.e., mean, minimum, and maximum) are computed for eight subregions (50 km interval) along the Tohoku coast and presented in Figure 6. The effects due to the buried fault plane are noticeable in the northern part of the Tohoku region, where complex topography due to ria coast exists, whereas the maximum inundation heights for the two cases are almost the same in the southern part of the Tohoku region, where topography is characterized as coastal plain. Figure 6 confirms the previous observations that the impact of top-edge depth variations can be significant for nearshore tsunami height.

Discussion

Both the parametric example and case study for the 2011 Tohoku tsunami highlight that the effects of varied top-edge depth parameters on vertical seabed deformation and tsunami

Table 1
Comparison of Displaced Volume of Water (in km^3) in the Trench Zone, Down-Dip Zone, Outer Fault-Plane Zone, and Combined Zone for Two Cases with $H_{top} = 0$ km and $H_{top} = 5$ km

Case	Trench Zone	Down-Dip Zone	Outer Fault-Plane Zone	Combined Zone
$H_{top} = 0$ km	84.743 (27.56%)*	133.980 (43.57%)*	88.784 (28.87%)*	307.508
$H_{top} = 5$ km	90.314 (26.32%)*	133.575 (38.93%)*	119.270 (34.76%)*	343.158
Difference	5.570 (6.57%)†	−0.405 (−0.30%)†	30.485 (34.34%)†	35.651 (11.59%)†

*Percentage with respect to the total displaced volume of water in the combined zone for the same case.
†Percentage of the difference of displaced volume of water between the two cases with respect to the displaced volume of water for the case with $H_{top} = 0$ km.

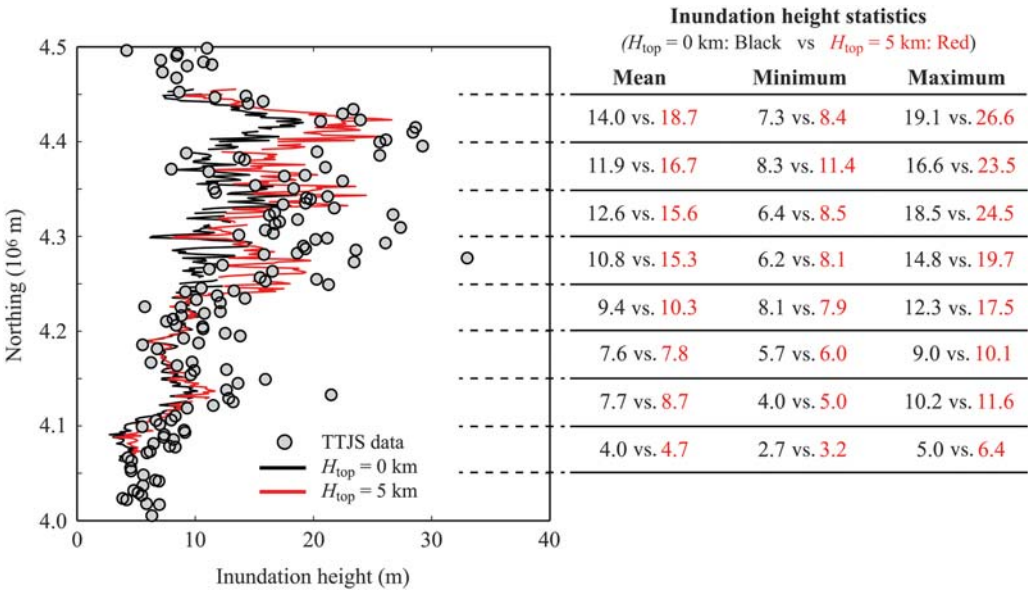

Inundation height statistics
(H_{top} = 0 km: Black vs H_{top} = 5 km: Red)

Mean	Minimum	Maximum
14.0 vs. 18.7	7.3 vs. 8.4	19.1 vs. 26.6
11.9 vs. 16.7	8.3 vs. 11.4	16.6 vs. 23.5
12.6 vs. 15.6	6.4 vs. 8.5	18.5 vs. 24.5
10.8 vs. 15.3	6.2 vs. 8.1	14.8 vs. 19.7
9.4 vs. 10.3	8.1 vs. 7.9	12.3 vs. 17.5
7.6 vs. 7.8	5.7 vs. 6.0	9.0 vs. 10.1
7.7 vs. 8.7	4.0 vs. 5.0	10.2 vs. 11.6
4.0 vs. 4.7	2.7 vs. 3.2	5.0 vs. 6.4

Figure 6. Tsunami inundation height profiles along the Tohoku coast by considering two cases, $H_{top} = 0$ km and $H_{top} = 5$ km, in comparison with the Tohoku Tsunami Joint Survey (TTJS) data. The inundation statistics shown in the figure are calculated at 50 km intervals as indicated by the dotted lines.

simulation results can be significant. When the fault plane is positioned at a shallow depth, unphysical, large peak vertical deformation is generated along the top edge of the dipping fault. In tsunami modeling, short-wavelength as well as long-wavelength components are excited due to the additional uplift. The uplifted water outside of the fault-rupture plane also generates large tsunami waves. The 2011 Tohoku tsunami provides empirical evidence for the importance of these effects. Situations similar to the 2011 Tohoku tsunami may be applicable to other tsunamigenic earthquakes in which a large slip occurs on a gently dipping fault plane at a shallow depth. For instance, the results presented in this study are relevant for carrying out tsunami sensitivity analysis for the anticipated Nankai–Tonankai earthquake, in which the seabed surface rupture is assumed while its slip distribution is only loosely constrained by available seismological data.

Importantly, the results shown in this study have implications on how tsunami inversion should be carried out and how developed source models should be interpreted. This is a critical issue for tsunami-hazard and risk assessments due to future earthquakes. For the case of the Satake *et al.* model for the 2011 Tohoku tsunami, the fault geometry for tsunami inversion was selected in advance; that is, the depth of the top of the fault plane is set to zero and the dip of 8° at the shallowest part was adopted (dip angle gradually steepens with depth). Through tsunami inversion, the maximum slip of 69 m (cumulative) was estimated. If the surface rupture to seabed is not assumed (e.g., top-edge depth of 3–5 km, which is typically adopted by other source inversion studies; Goda *et al.*, 2014), lower values of slip near the trench might have been estimated because the buried fault-plane case generates additional tsunami waves from the outer fault-plane region (as shown in Fig. 2b, there is a complex trade-off and interaction between inverted parameters and geometrical parameters).

It is also important to clarify that as long as internal consistency between inversion and forward analyses is maintained (i.e., a combination of numerical methods, bathymetry/elevation/roughness data, and calibration data), the effects of different assumptions, such as top-edge depth, on the simulated tsunami wave characteristics will not be so dramatic. However, in situations in which various source models are used for forward modeling of tsunami waves, such internal consistency may not be achievable. For instance, it is difficult to use exactly the same numerical methods and data, as employed in inversion studies, when tsunami waves are predicted by adopting a range of tsunami source models.

An important message from this study is that one should be cautious in applying Okada equations (and similar analytical formulas) when a large slip patch at a shallow depth close to the sea bottom is indicated in the source model, because unphysical vertical deformation that is estimated by Okada equations may be mapped onto inverted source characteristics. Therefore, further investigations on the effects of adopting different fault geometry parameters on the estimated slip distribution are worthwhile.

Data and Resources

A report on tsunami assessment methods for nuclear power plants in Japan by the Japan Society of Civil Engineers (2002) is available at http://committees.jsce.or.jp/ceofnp/system/files/JSCE_Tsunami_060519.pdf (last accessed April 2015). A report on megathrust earthquake models for the Nankai trough, Japan, by the Central Disaster Management

Council (2012) is available at http://www.bousai.go.jp/jishin/nankai/taisaku/pdf/20120829_2nd_report01.pdf (last accessed April 2015). The bathymetry and elevation data for the Tohoku region were provided by the Cabinet Office of Japanese Government. The runup and inundation survey data were obtained from the 2011 Tohoku Tsunami Joint Survey Group (http://www.coastal.jp/tsunami2011/; last accessed April 2015).

Acknowledgments

This work was supported by the Engineering and Physical Sciences Research Council (EP/M001067/1). The author is grateful to Martin Mai, Nobuhito Mori, and Tomohiro Yasuda for inspiring discussions on the subject. The author is grateful to two anonymous reviewers for their insightful comments and suggestions.

References

Federal Emergency Management Agency (2008). *Guidelines for Design of Structures for Vertical Evacuation from Tsunamis*, FEMA P646, Washington, D.C.

Geist, E. L. (2002). Complex earthquake rupture and local tsunamis, *J. Geophys. Res.* **107,** doi: 10.1029/2000JB000139.

Geist, E. L., and S. L. Bilek (2001). Effect of depth-dependent shear modulus on tsunami generation along subduction zones, *Geophys. Res. Lett.* **28,** 1315–1318.

Glimsdal, S., G. K. Pedersen, C. B. Harbitz, and F. Løvholt (2013). Dispersion of tsunamis: Does it really matter? *Nat. Hazards Earth Syst. Sci.* **13,** 1507–1526.

Goda, K., P. M. Mai, T. Yasuda, and N. Mori (2014). Sensitivity of tsunami wave profile and inundation simulations to earthquake slip and fault geometry for the 2011 Tohoku earthquake, *Earth Planets Space* **66,** no. 105, doi: 10.1186/1880-5981-66-105.

Goto, C., Y. Ogawa, N. Shuto, and F. Imamura (1997). *Numerical Method of Tsunami Simulation with the Leap-Frog Scheme (IUGG/IOC Time Project), IOC Manual No. 35*, United Nations Educational, Scientific and Cultural Organization, Paris, France.

Gusman, A. R., Y. Tanioka, S. Sakai, and H. Tsushima (2012). Source model of the great 2011 Tohoku earthquake estimated from tsunami waveforms and crustal deformation data, *Earth Planet Sci. Lett.* **341/344,** 234–242.

Kajiura, K. (1963). The leading wave of a tsunami, *Bull. Earthq. Res. Inst. Univ. Tokyo* **41,** 535–571.

Kawai, H., M. Satoh, K. Kawaguchi, and K. Seki (2013). Characteristics of the 2011 Tohoku tsunami waveform acquired around Japan by NOWPHAS equipment, *Coast. Eng. J.* **55,** no. 03, 1–27.

Løvholt, F., G. K. Pedersen, S. Bazin, D. Kuhn, R. E. Bredesen, and C. B. Harbitz (2012). Stochastic analysis of tsunami runup due to heterogeneous coseismic slip and dispersion, *J. Geophys. Res.* **117,** C03047, doi: 10.1029/2011JC007616.

Mai, P. M., and G. C. Beroza (2002). A spatial random field model to characterize complexity in earthquake slip, *J. Geophys. Res.* **107,** no. B11, doi: 10.1029/2001JB000588.

McCloskey, J., A. Antonioli, A. Piatanesi, K. Sieh, S. Steacy, S. Nalbant, M. Cocco, C. Giunchi, J. D. Huang, and P. Dunlop (2008). Tsunami threat in the Indian Ocean from a future megathrust earthquake west of Sumatra, *Earth Planet Sci. Lett.* **265,** 61–81.

Mori, N., T. Takahashi, T. Yasuda, and H. Yanagisawa (2011). Survey of 2011 Tohoku earthquake tsunami inundation and run-up, *Geophys. Res. Lett.* **38,** doi: 10.1029/2011GL049210.

Murata, S., F. Imamura, K. Katoh, Y. Kawata, S. Takahashi, and T. Takayama (2010). *Tsunami: To Survive from Tsunami*, World Scientific Publishing, Hackensack, New Jersey.

Murotani, S., K. Satake, and Y. Fujii (2013). Scaling relations of seismic moment, rupture area, average slip, and asperity size for $M \sim 9$ subduction-zone earthquakes, *Geophys. Res. Lett.* **40,** 5070–5074.

Okada, Y. (1985). Surface deformation due to shear and tensile faults in a half-space, *Bull. Seismol. Soc. Am.* **75,** 1135–1154.

Satake, K., Y. Fujii, T. Harada, and Y. Namegaya (2013). Time and space distribution of coseismic slip of the 2011 Tohoku earthquake as inferred from tsunami waveform data, *Bull. Seismol. Soc. Am.* **103,** 1473–1492.

Tanioka, Y., and K. Satake (1996). Tsunami generation by horizontal displacement of ocean bottom, *Geophys. Res. Lett.* **23,** 861–864.

Yamazaki, Y., Z. Z. Kowalik, and K. F. Cheung (2009). Depth-integrated, non-hydrostatic model for wave breaking and run-up, *Int. J. Numer. Meth. Fluid.* **61,** 473–497.

Yamazaki, Y., T. Lay, K. F. Cheung, H. Yue, and H. Kanamori (2011). Modeling near-field tsunami observations to improve finite-fault slip models for the 11 March 2011 Tohoku earthquake, *J. Geophys. Res.* **38,** L00G15, doi: 10.1029/2011GL049130.

Civil Engineering
University of Bristol
Queen's Building
University Walk
Bristol, BS8 1TR, United Kingdom
katsu.goda@bristol.ac.uk

Manuscript received 2 April 2015;
Published Online 25 August 2015